Study of Silicon Thickness Optimization for LSST

P. O'Connor[a*], V. Radeka[a], D. Figer[b], J.G. Geary[c], D.K. Gilmore[d], J. Oliver[e], C.W. Stubbs[f], P.Z. Takacs[a], J.A. Tyson[g]

[a]Brookhaven National Laboratory, Upton, NY, USA 11973-5000; [b]Space Telescope Science Institute, 3700 San Martin Drive, Baltimore, MD 21218; [c]Harvard-Smithsonian Center for Astrophysics, 60 Garden St., Cambridge MA 02138; [d]Stanford Linear Accelerator Center, Stanford, CA; [e]Harvard University, Laboratory for Particle Physics and Cosmology, 18 Hammond St., Cambridge, MA 02138; [f]Department of Physics, Harvard University, 17 Oxford St., Cambridge, MA, USA 02138; [g]University of California, Davis, CA 95616

ABSTRACT

Sensors for the LSST camera require high quantum efficiency (QE) extending into the near-infrared. A relatively large thickness of silicon is needed to achieve this extended red response. However, thick sensors degrade the point spread function (PSF) due to diffusion and to the divergence of the fast f/1.25 beam. In this study we examine the tradeoff of QE and PSF as a function of thickness, wavelength, temperature, and applied electric field for fully-depleted sensors. In addition we show that for weakly absorbed long-wavelength light, optimum focus is achieved when the beam waist is positioned slightly *inside* the silicon.

Keywords: LSST, quantum efficiency, point spread function, overdepletion

1. INTRODUCTION

The LSST focal plane is the largest ever proposed for an astronomical instrument. The demands of the science to be done and the nature of the cadence and very wide field preclude the use of any existing imager, so a custom device must be developed. Both CCD and PIN-CMOS imagers are being considered. Of central importance are high quantum efficiency (QE) extending into the near infrared and small point spread function (PSF). To achieve high QE in the near-IR, the sensor must be thick because the absorption depth of silicon increases rapidly in this wavelength range. However, increasing detector thickness degrades the spatial resolution of the sensor due to two effects. Diffusion of the photogenerated charge increases because of the longer transit time to the collecting electrode. Thick sensors also require sufficient substrate bias to fully deplete the device; otherwise, lateral diffusion in the undepleted field-free region severely degrades the PSF. A second cause of PSF broadening results from the fast focal ratio of the LSST optics (f/1.2). For red wavelengths where the absorption length is comparable to or greater than the sensor thickness, the light becomes defocused before it is fully absorbed, further broadening the PSF.

This study is organized as follows:
- Section 2: quantum efficiency as a function of wavelength, temperature, and thickness
- Section 3: point spread function due to diffusion and beam divergence
- Section 4: optimization of thickness using point source limiting magnitude as a figure of merit

2. QUANTUM EFFICIENCY

We distinguish here between internal QE, the device efficiency after light enters the detector, and total QE, which includes reflection losses due to dielectric mismatch. Our focus in this paper is on internal QE.

2.1 Absorption length in silicon

The absorption length is defined as the depth at which the light intensity falls to 1/e of the original incident intensity. We adopt the empirical model of Rajkanan [1] to find the absorption length of silicon as a function of wavelength and temperature [Fig. 1]. Note that absorption length increases rapidly for photon energies near the band gap of silicon (about 1000 nm). There is also a strong increase of absorption with temperature, especially in the red, since transitions near the indirect band gap must be phonon-assisted to conserve momentum.
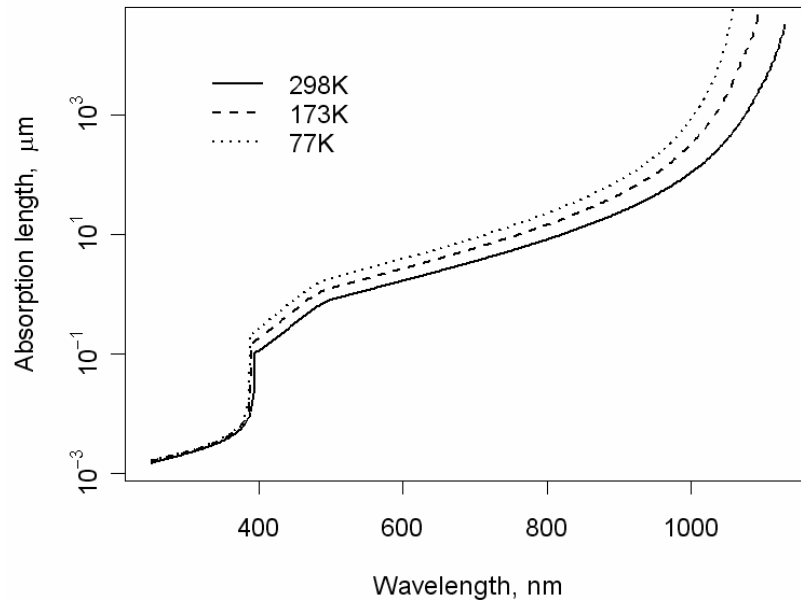

Figure 1. Absorption length in silicon, after Reference [1]. Long-wavelength absorption length is strongly temperature-dependent.

2.2 Quantum efficiency

The LSST specifications for total quantum efficiency are as follows [2]:

Table 1. LSST quantum efficiency requirements

Wavelength	Quantum Efficiency	
	Allowable	Target
400 nm	55%	60%
600	80	85
800	80	85
900	60	85
1000	25	45

Sensor quantum inefficiency arises from reflection loss, incomplete charge collection (usually a negligible effect), and incomplete light absorption. In this study we only model the effect of incomplete absorption. The reflectivity properties of the final LSST sensors will depend on the antireflection coating used on the illuminated surface and on the interface properties on the opposite (charge-collecting) side, which are not known at this point. Charge collection is expected to be near unity over most of the wavelength range, but surface defects will cause a falloff toward the blue end where absorption takes place very near the surface. For the red and near-IR region, reflection losses will reduce the QE and multiple internal reflections will cause interference fringes in the optical response (although for thick sensors and low f-number the fringing is reduced). Hence the internal quantum efficiency reported here should be considered an upper limit.

Figure 2 shows the modeled quantum efficiency at longer wavelengths for different sensor thicknesses at a temperature of –100°C.
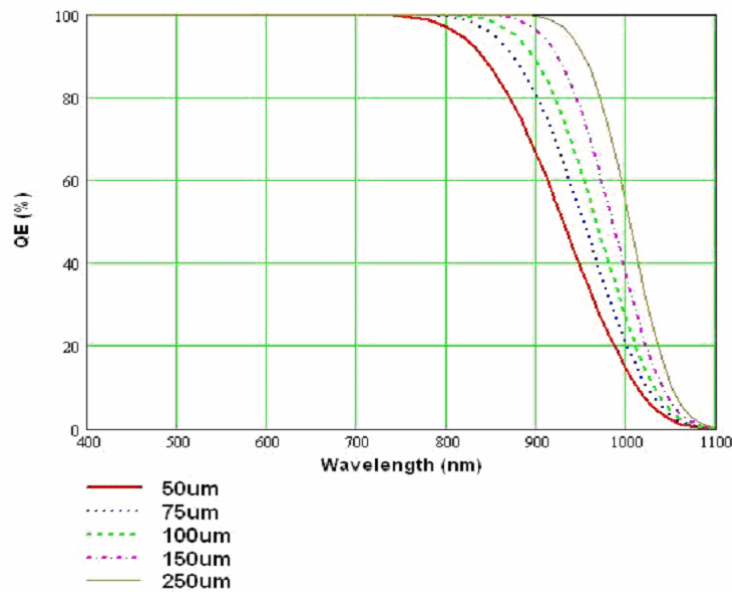

Figure 2. Internal quantum efficiency at 173K as a function of wavelength for several sensor thicknesses. Reflection and charge collection losses not modeled.

For the critical 1000-nm wavelength, the dependence of internal QE on temperature and sensor thickness is shown by the contour plot in Figure 3. If the focal plane is operated at a temperature of -100C (choice of temperature is dependent on dark current characteristics), a silicon thickness of no less than 100μm will be needed to meet the LSST minimum acceptable QE at 1000nm. Note that at λ = 1000nm the relative QE varies by about 1% per degree C.
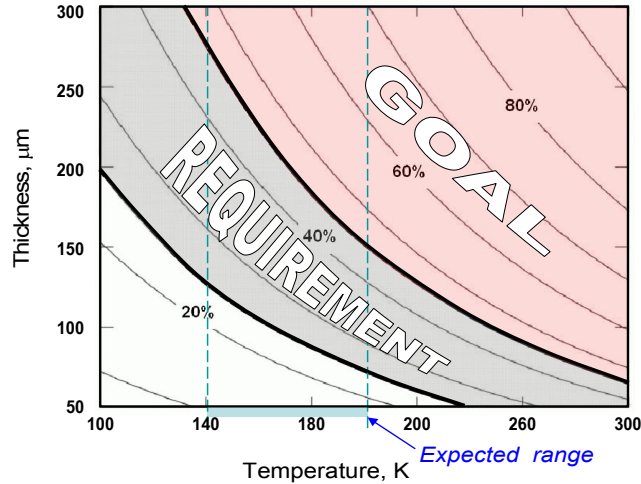
Figure 3. Internal QE at $\lambda = 1000$ nm (solid contours) as a function of sensor thickness and temperature.

3. POINT SPREAD FUNCTION

Several of the science missions of the LSST depend on its ability to resolve faint point sources. The signal-to-noise ratio for a point source depends inversely on the PSF, since the smaller the area over which the image is spread, the less sky noise is acquired with the signal. Contributions to the PSF come from aberrations of the telescope optics (including fabrication and alignment tolerances), atmospheric seeing at the site, and detector contributions. The LSST specification for the detector contribution to the point spread function is [2]:

	Allowable	Target
Pixel FWHM (charge spreading)	< 10 μm	< 7.5 μm

(In subsequent discussion of we will assume an approximately Gaussian PSF, for which the allowable and target rms values are 4.25 and 3.19μm respectively.)

The LSST plate scale is 50.9μm per arcsecond, and the pixel size is 10μm.

At short wavelengths, the main contribution to charge spreading comes from diffusion. At near-IR wavelengths, there is additional broadening due to the divergent "cone" of light that enters the sensor. The light becomes progressively defocused and the deeper the point of absorption, the wider the effective spot size. These effects will be analyzed in the next two sections.

3.1 Charge Diffusion

Visible photons are absorbed in a thin layer near the illuminated (back) side of the sensor and the resulting charges move to the electrode side under the influence of the applied electric field. To achieve small point spread function it is important to apply a bias that will deplete the entire sensor thickness. If not, there will be a field-free, neutral layer of thickness d_{FF} near the illuminated face of the sensor. Charges generated in the field-free region diffuse isotropically and will have a profile of rms width $\approx d_{FF}$ when they encounter the electric field that sweeps them to the collecting side of the sensor. The bias needed to fully deplete a device of thickness d is

$$V_{depl} = \frac{qd^2N}{2\varepsilon_{Si}}, \tag{1}$$

where N is the density of donor or acceptor dopants in the substrate, ε_{Si} is the permittivity of silicon, and q is the electron charge. For high-resistivity silicon with a dopant density in the range of 10^{12}cm^{-3}, about 10V is required to deplete a thickness of 100μm. In terms of material resistivity, for a 5kΩ-cm substrate ~7V is required in n-type and ~20V in p-type for full depletion.

Using a one-dimensional approximation, the electric field in an overdepleted sensor of thickness d varies linearly with distance z from the illuminated surface as

$$E(z) = E_{\min} + 2V_{depl}z/d^2, \qquad (2)$$

where $E_{min} = (V_{op} - V_{depl})/d$ is the field at the illuminated surface, V_{op} is the operating voltage, and V_{depl} is the depletion voltage given by Eq. (2). The rms diffusion for carriers traversing the full sensor thickness is

$$\sigma_D = \sqrt{2Dt_{dr}}, \qquad (3)$$

where $t_{dr} = \int_0^d dz/v$ is the drift time of carriers moving with velocity v in the electric field.

In an overdepleted sensor and high resistivity material (ρ > 10000Ω-cm) the velocity is nearly constant. Assuming initially a constant mobility, the drift velocity is given by $v=\mu E_{av} = \mu V_{appl}/d$, where μ is the mobility of minority carriers and V_{op} is the applied voltage across the sensor. Then using the Einstein relation $D=kT\mu/q$ and (3) we find a simplified expression for the diffusion

$$\sigma_D \approx \sqrt{\frac{2kT}{qE}} = d\sqrt{\frac{2kT}{qV_{op}}}. \qquad (4)$$

Equation (4) does not depend on any silicon properties and is useful for first-order estimates of diffusion, but only in over depletion, $V_{op}/V_{depl}>2$.

In the general case the diffusion calculation has to take into account the non-uniform electric field (2), as well as field-dependent carrier velocity and field-dependent longitudinal and transverse diffusion coefficients and their temperature dependence. In the special case of interest to LSST, the sensors will have to be operated well overdepleted and then the effects of the slightly non-uniform electric field become negligible. However, the carrier velocity saturation effects are important and have to be taken into account. There is an increase in diffusion due to longer carrier drift time than expected in the constant mobility case, while there is a compensating decrease in the transverse diffusion coefficient due to the streamlining effect of the electric field on the carriers in random + drift motion. *These effects have been included in all the calculations of the expected diffusion contribution to the PSF discussed in the remainder of this study.* The velocity effects on diffusion will be discussed in a separate note. For a temperature of 173K and 5kV/cm the two opposing effects result in an overall diffusion increase of a factor of about 1.15 for electrons (1.3 for holes) compared to the simple approximation (4).

Long-wavelength light generates carriers at varying depths in the silicon, so their diffusion has to be weighted by the absorption probability:

$$\sigma_D(\lambda) = \frac{\int_0^d e^{-z/l_{abs}(\lambda)}\sigma_D(z)dz}{\int_0^d e^{-z/l_{abs}(\lambda)}dz}, \qquad (5)$$

where $\sigma_D(z)$ is the diffusion experienced by a carrier generated at a distance z from the entrance window of a sensor whose total thickness is d.

Figure 4 shows the PSF contours for high-resistivity p-type silicon on the thickness-voltage plane, with the effects of high and nonuniform electric field taken into account. Note that the voltage required to meet the LSST PSF target increases as the *square* of the silicon thickness, and is about four times greater than the full-depletion voltage for high-

resistivity material. For silicon with resistivity in this range, the rms diffusion exhibits a temperature coefficient of 0.007μm/°C.

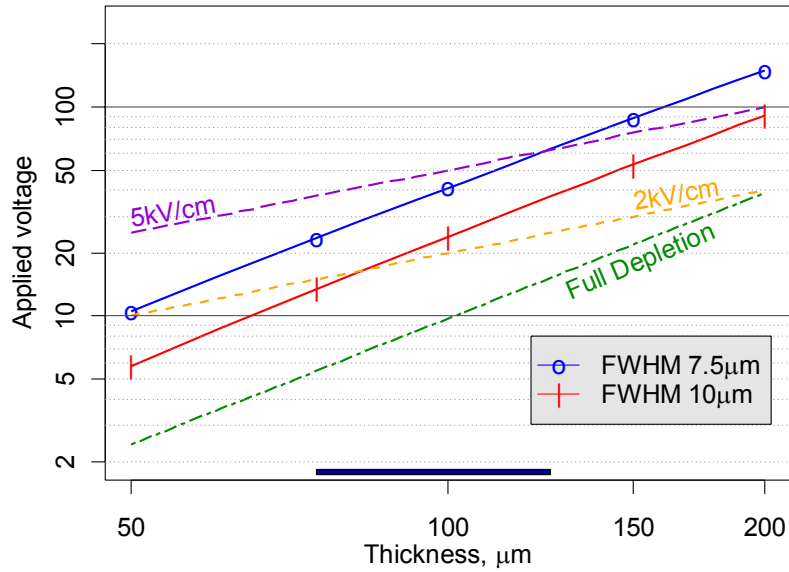Figure 4. Diffusion contours for short-wavelength light in p-type silicon, 10 kΩ-cm, at 173K. Dashed lines show average electric fields and the full depletion voltage. Carrier velocity saturation effects have been included in the diffusion calculation. The LSST *acceptable* is PSF = 10μm FWHM (4.25μm rms), the target is PSF = 7.5μm (3.2μm rms).

3.2 PSF broadening due to divergent optical beam in silicon

In a low-f number optical system like LSST, light is incident on the sensor at large angles from the normal. Figure 5 shows an optical raytrace result from the LSST f/1.2 configuration. Because of the high index of refraction of silicon, the light "cone" has a smaller half-angle inside the silicon than in air. The lower half of the figure shows the absorption of light of two wavelengths. For long wavelengths where the light absorption length l_{abs} is much greater than the sensor thickness, the light is absorbed almost uniformly, while shorter wavelength light is strongly absorbed at the surface.
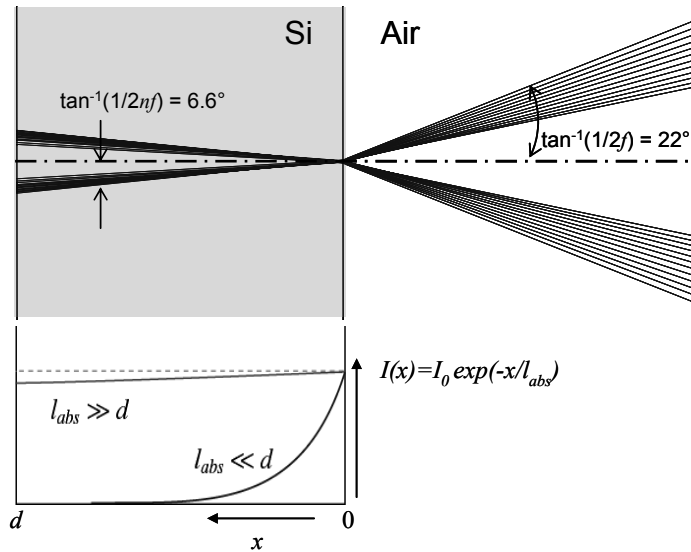
Figure 5. Optical raytrace showing refraction and absorption of light entering the silicon sensor. Light is incident from the right and focus is at the sensor illuminated surface.

Two methods were used to study the effect of beam divergence on PSF.

3.2.1 Raytrace method

Monte-Carlo simulations were performed for absorption lengths of 2, 10, 50, 100, 200, and 300 μm and for sensor thicknesses from 50 to 250 μm. For each configuration, ten thousand rays were traced into a thick silicon layer and the depth of conversion was selected according to the appropriate exponential probability distribution. The resulting ionization distribution was then projected onto the collecting surface, with the effect of diffusion optionally included based on the drift distance of each electron and using the expressions developed in subsection 3.1.

This method can also be used to study the optimum position of the focal plane. Because of the weak absorption at long wavelengths, the projected charge distribution on the electrode side of the sensor can be made smaller by displacing the focal plane in the direction of the incoming light. Figure 6 illustrates the effect. When the sensor is displaced towards the incoming rays, long-wavelength light comes to a focus *within* the body of the sensor and the projection of the generated charge forms a smaller spot. The amount of focal plane displacement is highly sensitive to wavelength and also depends on temperature.
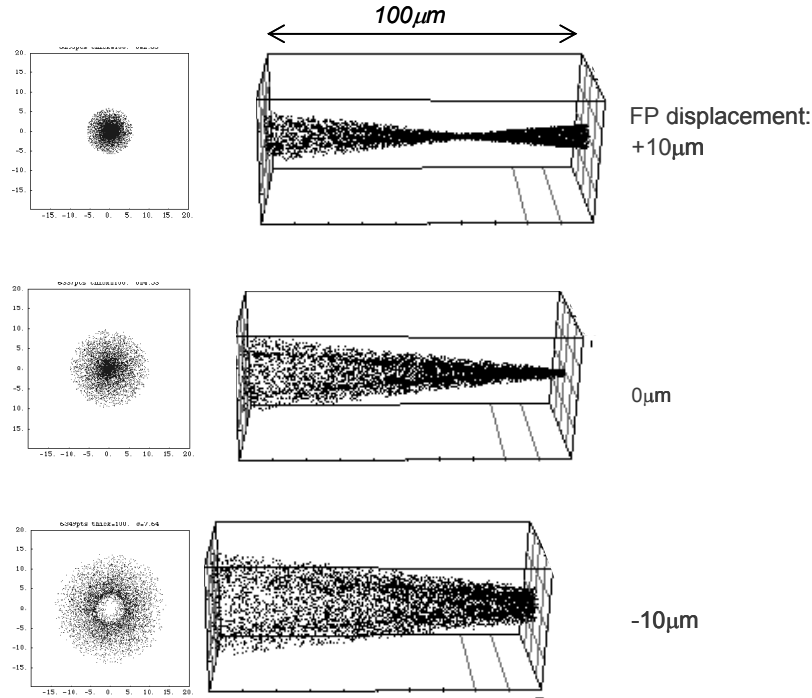
Figure 6. Absorption of long-wavelength light in a 100µm-thick sensor. Focal plane position shown displaced by 0, and ±10 microns from best short-wavelength focus. Spot diagrams (with no diffusion) shown on the left.

3.2.2 Geometrical method

An analytic estimate of the PSF broadening from beam divergence can also be made, by weighting the radius of the light cone by the absorption probability at a depth z in the sensor. The telescope images a point-source to a spot modeled by a Gaussian profile of width σ_{tel}. The silicon sensor is initially introduced with its entrance face at $z=0$ and refracts the light as shown in Fig. 5; positive and negative displacements of the sensor produce light distributions as shown in Fig. 6. We model the geometric width of the light spot as a function of the displacement δ and the distance from the entrance face z as:

$$\sigma(\delta, z) = \sigma_{tel} + \frac{|z - n\delta|}{2nf}, \quad \delta > 0$$

$$= \sigma_{tel} + \frac{|\delta|}{2f} + \frac{z}{2nf}, \quad \delta < 0 \tag{6}$$

where n is the refractive index of silicon and f is the focal ratio of the telescope. Equation (6) accounts for the increased width of the beam at the sensor surface and the appropriate converging and diverging light "cones" in the sensor. Following Groom [3,4] we form the weighted average of the beam width over the exponential absorption through the sensor:

$$\sigma_{div}^2(\delta) = \frac{\int_0^d \sigma^2(\delta, z) e^{\frac{-z}{l_{abs}}} dz}{\int_0^d e^{\frac{-z}{l_{abs}}} dz} \tag{7}$$

The geometry is illustrated in Figure 7. This method was found to give very good agreement with the raytrace results over a range of thickness, absorption length, and focal displacement.
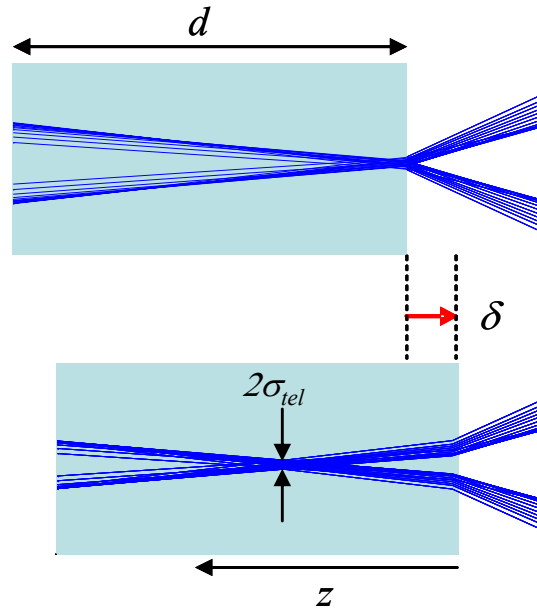

Figure 7. Geometrical model of the divergence PSF. Light is incident from the left and silicon region is shown shaded. Top: nominal focus position. Bottom: sensor displaced by δ towards the incident light.

3.3 Combined effect of diffusion and beam divergence

The models of section 3.1 and 3.2 can be combined to give an estimate of the PSF for various sensor configurations and bias conditions. Figure 8 shows how the PSF behaves for a 100μm-thick sensor as the focal plane is is displaced. Effects of diffusion and divergence are included. At low electric field, diffusion dominates and the short-wavelength PSF does not meet the LSST requirement. Raising the electric field to 5 kV/cm brings down the diffusion and the minimum PSF exceeds the LSST target for all wavelengths. The focal plane has to be displaced about 15μm to produce the minimum PSF in the Y-band (970 – 1060nm).

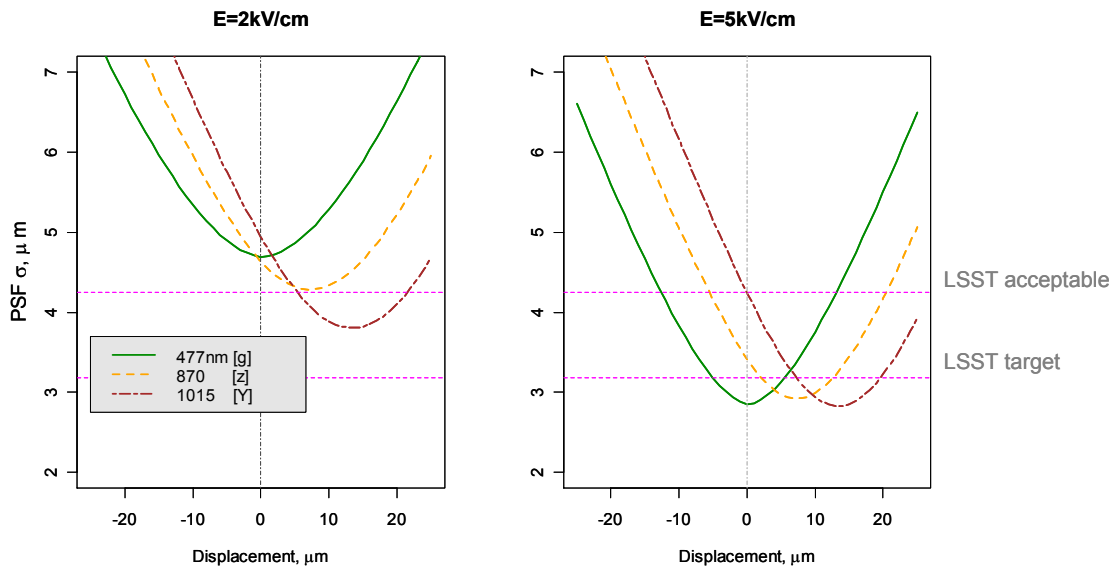Figure 8. PSF rms vs. focal plane displacement for two values of electric field. Thickness 100μm, resistivity 10 kΩ-cm p-type, temperature 173K.

Figure 9 shows the PSF as a function of thickness, with the focal plane position optimized at each thickness and wavelength. Three values of electric field are shown. To meet the LSST *acceptable* specification, the sensor thickness must be less than 175μm and a field of at least 5 kV/cm must be applied. The LSST *target* requires a sensor no thicker than 125μm.
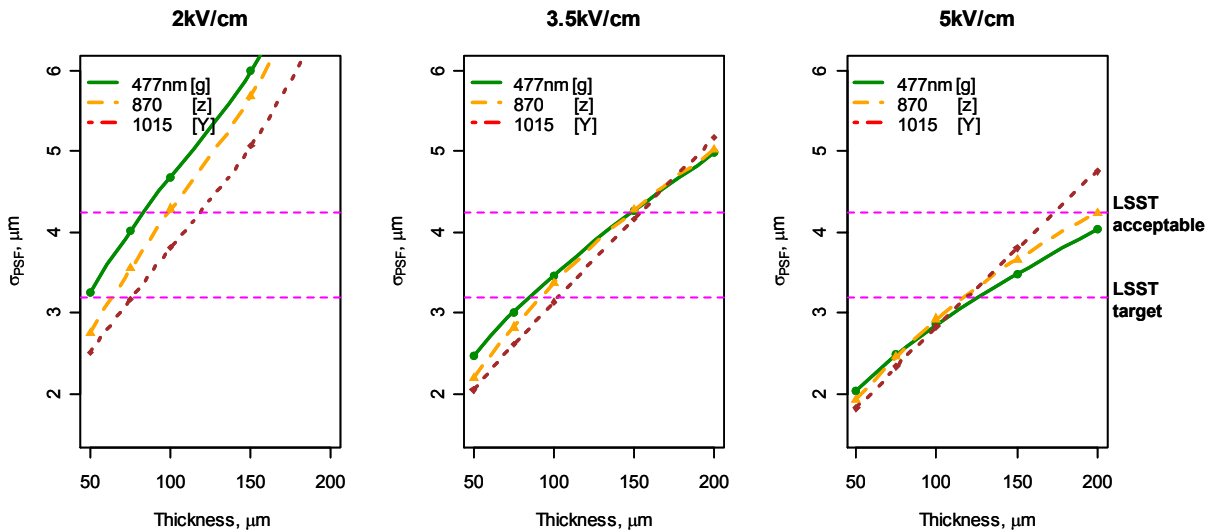
Figure 9. PSF rms vs. thickness for three values of electric field. Effects of diffusion and divergence included, with focal plane position optimized at each thickness and wavelength. Temperature 173K, resistivity 10kΩ-cm p-type. Carrier velocity saturation effects have been included in the diffusion calculation.

4. DETECTION LIMIT

The signal-to-noise ratio for point source detectability can be written as

$$SNR = \frac{QR_*t}{\sqrt{QR_*t + n_{pix}[QR_{sky}t + R_{dark}t + RN^2]}}$$ (8)

where Q is the quantum efficiency, R_* and R_{sky} are the source and sky flux at the detector respectively, n_{pix} is the effective number of pixels that contain most of the source flux, R_{dark} is the dark current generation rate, RN is the read noise, and t is the exposure time. n_{pix} can be defined as $\pi r^2/A_{pix}$, where r = radius around the source containing most of the light and A_{pix} is the pixel area. For Gaussian PSF, the optimum SNR occurs at $r = 1.585\sigma$, where σ is the rms width of the PSF. In the faint source limit the signal-to-noise is thus proportional to $\dfrac{\sqrt{Qt/R_{sky}}}{\sigma_{PSF}}$. We have seen that in general Q and σ_{PSF} both increase with sensor thickness, especially at near-IR wavelengths.

The point source figure of merit (8) (or equivalently the limiting magnitude for which the S/N exceeds a desired threshold) can be calculated after making some assumptions about the LSST site, optics, and filters. Table 2 shows the telescope and sensor parameters and Table 3 gives a set of five possible filter choices for LSST [5].

Table 2. LSST telescope and sensor parameters.

Primary mirror diameter	8.4m
Secondary obscuration	61%
Mirror transmission per surface	97%
Filter transmission per surface	97%
Exposure time	15s
Sensor dark rate	4 e⁻/pixel/s
Sensor read noise	10e⁻/read

Table 3. LSST filter set, and sky brightness in each band [5,6]

Filter	lower cutoff	upper cutoff	Sky brightness
g	402	552	22.3
r	552	691	21.2
i	691	818	20.0
z	818	922	19.1
Y	970	1060	18.4
	nm	nm	mag/arcsec²

For each sensor thickness, the expressions for QE and PSF developed in Sections 2 and 3 were averaged over the filter bandwidths and the limiting magnitude for detectability at the level of SNR=10 was calculated from Eq. (8). For red wavelengths, we used the PSF at best focus as discussed in Section 3.3. The results are shown in Fig. 10 and Fig. 11.
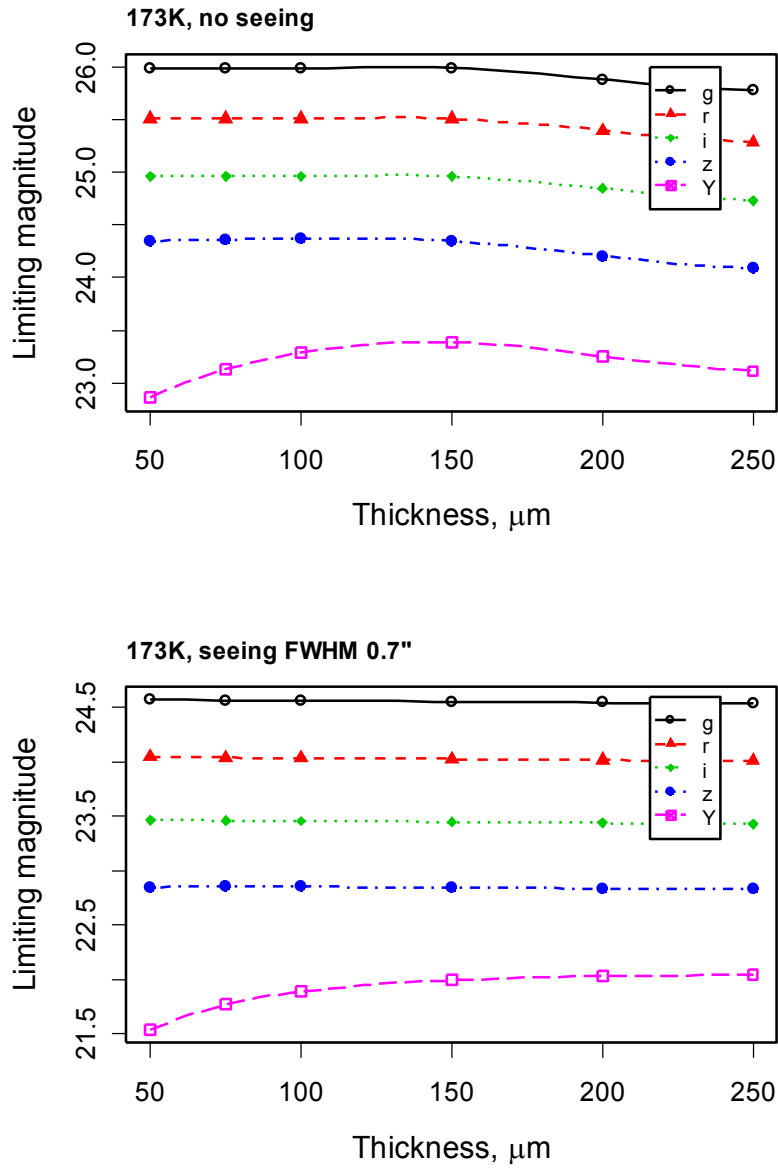
Figure 10. Limiting magnitude (S/N = 10) for 15-second LSST exposures, for the filter set shown in Table 3. Sensor operating temperature 173K; substrate 10kΩ-cm p-type; average electric field 5 kV/cm; focal plane position adjusted for best focus in each band. Reflection losses at sensor and atmospheric extinction not included. Top: Atmospheric seeing not included; Bottom: including seeing of 0.7" FWHM.
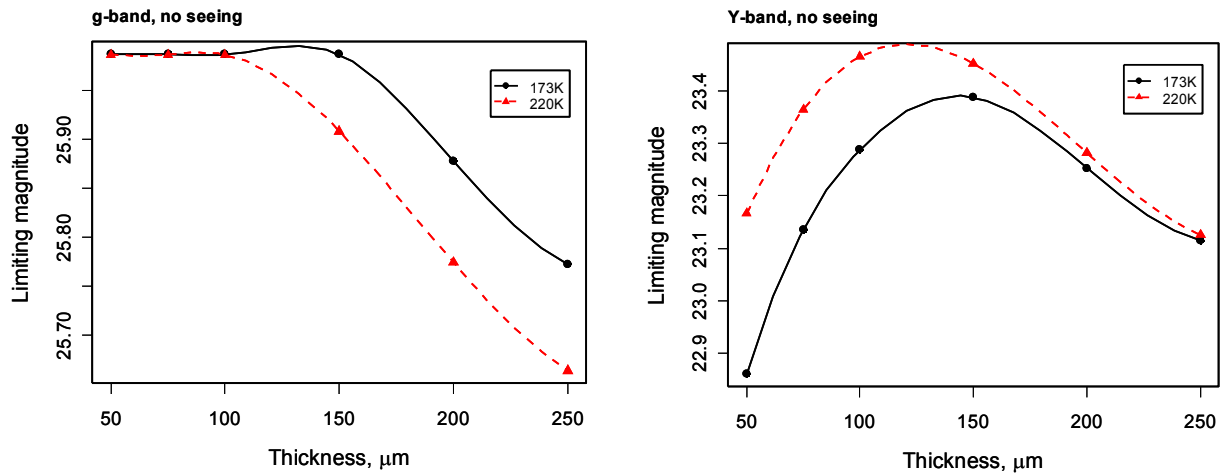
Figure 11. Limiting magnitude vs. thickness compared at two temperatures. Left: *g*-band. Right: *Y*-band. Same detector parameters as Fig. 10.

5. CONCLUSIONS

We have studied the dependence of LSST sensors on silicon thickness. Since thicker sensors have better red quantum efficiency but poorer point spread function, a compromise thickness must be chosen. The quantum efficiency has been calculated based on the known absorption length of silicon as a function of wavelength and temperature. PSF was estimated from knowledge of the high-field transport properties of carriers, and by Monte-Carlo modeling of light conversion in the sensor. The important conclusions are:

- At least 100μm thickness is needed to reach the LSST requirement for 25% QE at λ = 1000nm.

- The sensor must have high resistivity and be biased well above full depletion to control the diffusion component of PSF.

- The fast focal ratio of LSST leads to an additional contribution to PSF at long wavelengths, due to the projection of the divergent cone of weakly-absorbed light.

- Because of beam divergence, there is a focus shift at long wavelengths where optimum focus is obtained with the sensor displaced in the direction of the incoming light.

- A sensor thickness of around 125 – 150μm gives the optimum 10σ detection limit in Y-band.

REFERENCES

1. K. Rajkanan et al., Sol. St. Electr. 22, 793-795 (1979).

2. R. Allsman et al., "The Large Synoptic Survey Telescope (LSST), A proposal for research and development and pre-construction engineering design", submitted to Dept. of Energy Jan. 20, 2006, Table 4.3.2-2 and Table 4.3.2-3.

3. D.E. Groom, "The red problem", LBL Internal Note, 31 October 1996. Available:
http://design.lbl.gov/ccd/papers/red_problem.ps.

4. D.E. Groom, "Update of depth of focus considerations for red light incident on a thick CCD in a fast optical system",
LBL Internal Note, 20 March 2002. Available: http://www-ccd.lbl.gov/depth_focus.ps.

5. R. Allsman, op. cit., Table 4.3.7-2.

6. A. Walker et al. "Night Sky Brightness at Cerro Pachon", 15 June 2004, NOAO newsletter #10. Available:
http://www.ctio.noao.edu/site/pachon_sky/.

DISCLAIMER